ELSEVIER

Colloids and Surfaces A: Physicochem. Eng. Aspects 220 (2003) 139–150

COLLOIDS AND SURFACES A

www.elsevier.com/locate/colsurfa

Adsorption and desorption kinetics of C_mE_8 on impulsively expanded or compressed air–water interfaces

Ya-Chi Lee [a], Kathleen J. Stebe [b], Hwai-Shen Liu [a], Shi-Yow Lin [c,*]

[a] *Department of Chemical Engineering, National Taiwan University, 1 Roosevelt Road, Sec. 4, Taipei 106, Taiwan*
[b] *Department of Chemical Engineering, Johns Hopkins University, 3400 North Charles Street, Baltimore, MD 21218, USA*
[c] *Department of Chemical Engineering, National Taiwan University of Science and Technology, 43 Keelung Road, Sec. 4, Taipei 106, Taiwan*

Received 9 May 2002; accepted 17 February 2003

Abstract

The adsorption kinetics of C_mE_8 ($m = 10$, 12, and 14) at an air–water interface are investigated. A pendant bubble is formed in aqueous surfactant solution and allowed to attain equilibrium. The bubble is then impulsively expanded or compressed with some change of area large enough to appreciably deplete or enrich the surface concentration and change the surface tension. The surfactant is then allowed to re-equilibrate. The surface tension evolution during this process is measured using video images of the pendant drop. The surface tension evolution is compared to mass transfer arguments. First, the re-equilibration of interfaces laden with $C_{14}E_8$ are studied. For compressed interfaces, surfactant must desorb to restore equilibrium. The surface tension rises more slowly than predicted by a diffusion-controlled evolution, implying that the re-equilibration is mixed diffusive-kinetic controlled. By analyzing the surface tension evolution in terms of a mixed kinetic-diffusive model, values for the kinetic constants for adsorption and desorption are found. These results are compared to those obtained previously for C_mE_8 ($m = 10$ and 12). For all of these molecules, the adsorption rate constant is similar ($\beta_1 = 5.6 \pm 1.0 \times 10^{-6}$ cm^3 (mol s)$^{-1}$). However, the desorption rate constant (α_1) varies strongly. Increasing m by 2 lowers the desorption rate constant α_1 by nearly a factor of 15. This is consistent with an increased resistance to re-immersion into water with the length of a hydrocarbon chain.

Keywords: Adsorption kinetics; Desorption; Dynamic surface tension; Kinetic rate constant; Pendant bubble method; Surface tension; Surfactant

1. Introduction

When an interface is formed in a surfactant solution, surfactants adsorb from the region immediately adjacent to the interface, locally depleting the solution and establishing a diffusion flux. Adsorption and diffusion kinetics therefore establish the surface tension evolution at early times. As

* Corresponding author. Tel.: +886-2-2737-6648, fax: +886-2-2737-6644.
E-mail address: ling@ch.ntust.edu.tw (S.-Y. Lin).

0927-7757/03/$ - see front matter
doi:10.1016/S0927-7757(03)00075-X

the interface approaches equilibrium, the desorptive and diffusive flux away from the interface must balance the fluxes toward the interface. Therefore, in general, both the rates of adsorption–desorption exchange and diffusion from the bulk toward the interface influence the surface tension evolution. Because the time required for a surfactant to diffuse from the bulk to the interface depends strongly on the bulk concentration, diffusion can be rate limiting at dilute concentrations, but occur over times that are comparable to adsorption–desorption kinetics at higher concentrations. This shift in controlling mechanism has been explored in dynamic surface tension studies of a variety of surfactant for adsorption to freshly formed bubbles in surfactant solutions. For example $C_{10}E_8$ and $C_{12}E_8$ were reported recently to have diffusion-controlled adsorption onto a freshly created air–water interface at dilute concentrations and a mixed diffusive-kinetic controlled adsorption at more elevated concentrations [1–4]. A transition between diffusion controlled and kinetically controlled adsorption has been also reported by Pan et al. [5] for $C_{12}E_6$ and Li et al. [6] for hexanoic acid and some ionic surfactants (SDS, MTAB, DoTAB, and DeTAB).

Experiments can be devised in which adsorption–desorption kinetics play an even more pronounced role in the surface tension evolution than in the high surfactant concentration data described above. For example, consider an interface in equilibrium with a surfactant solution. If that interface is rapidly compressed so that the surfactant on the interface is packed to a higher surface concentration, then desorption out of the interface must occur to allow the surfactant to re-equilibrate with the surrounding solution. Therefore, desorption kinetics from impulsively compressed interfaces should be slow enough to be rate limiting for surfactants whose tails are sufficiently long to have pronounced attractions in an adsorbed monolayer. If an interface that has come to equilibrium is impulsively expanded, the rates of adsorption can also be forced to play a strong role in the re-equilibration process. Adsorption is slower into a crowded interface. The timescale for diffusion is more rapid when delivering surfactant to an already populated interface, as less surfactant must be delivered in this case, and so adsorption depths are smaller. This combination of slower adsorption–desorption and faster diffusion fluxes allows kinetics barriers to be more apparent in these experiments than in adsorption to initially clean interfaces. A similar process named as transient relaxation had also been reported by Loglio et al. [7].

In this paper, impulsively expanded and compressed interfaces are used as a tool to study the mass transfer of the polyethoxylated surfactants $C_{14}E_8$. The diffusion coefficient is resolved from Lin et al. [8]. The rate constants for adsorption–desorption are found from the dynamic data by assuming a constant diffusion coefficient over the concentration range studied. These data are compared to data for $C_{10}E_8$ and $C_{12}E_8$, which re-equilibrate from suddenly compressed interfaces at rates slower than diffusion-controlled predictions [2,4].

2. Experimental measurements

2.1. Materials

Non-ionic surfactant $C_{14}E_8$ [octaethylene glycol mono *n*-tetradecyl ether ($C_{14}H_{29}(OCH_2CH_2)_8OH$) with purity $>99\%$, purchased from Nikko (Tokyo, Japan)] was used without modification. The water with which the aqueous solutions were made was purified via a Barnstead NANOpure water purification system, with the output water having a specific conductance of less than 0.057 $\mu\Omega^{-1}$ cm^{-1}.

2.2. Method: an impulsively deformed pendant bubble

A pendant bubble tensiometer enhanced by video digitization was employed for the measurement of dynamic surface tension of $C_{14}E_8$. The system has been described in detail in previous work [9], and is only briefly described here. The experiments were performed at 25.0 ± 0.1 °C. The bubble, approximately 2-mm diameter, was formed on the tip of a 16-gauge stainless steel

inverted needle (0.047 in. i.d.; 0.065 in o.d.). Sequential digital images of the bubble were then taken. The edge coordinates of the pendant bubble were compared to the theoretical shape derived from the classical Laplace equation to extract the surface tension from each pendant bubble image. By analyzing sequential images, the evolution of the surface tension with time can be measured. The accuracy and reproducibility of the surface tension measurements are approximately 0.1 mN m^{-1} [10].

For experiments to study the re-equilibration of interfaces compressed to pack surfactants above their equilibrium surface concentration, a bubble is formed and equilibrated in surfactant solution. Thereafter, enough air is allowed to leave the bubble through a solenoid valve to change the surface area abruptly (within 0.13 s) by 10–15%. The solenoid valve is then closed, and the bubble is left to re-equilibrate (over hundreds of seconds). Bubble images are recorded during the shrinkage of bubble, and after the solenoid valve has been closed. The images are analyzed to determine the bubble edge coordinates, the bubble volume, the bubble surface area, and the surface tension.

Four different bulk concentrations, $C = 1.0$, 1.3, 2.0, and 3.0 (10^{-9} mol cm^{-3}), were chosen for the experiment of surface compression. At each concentration, the experiments were performed several times.

In order to study the re-equilibration of a rapidly expanded interface, air is injected into an equilibrated pendant bubble by opening the solenoid valve to allow the influx of air by a syringe pump. The surface area is rapidly increased between 10 and 55% over 1.3 s and the valve is closed. The expansion of the bubble interface dilutes the surface concentration, causing surfactants to adsorb to restore equilibrium, typically over roughly 10^3 s. The relaxation of surface tension to restore equilibrium is monitored via the sequential digital images.

The window bulk concentration suitable for the expansion experiment is narrow. Solution of $C = 2.0 \times 10^{-9}$ mol cm^{-3} was chosen in this work. When C is too dilute, the rise of surface tension is only a few mN m^{-1} and is not significant enough. However as C is too high, the re-equilibration timescale becomes too rapid and the mass transfer during the expansion becomes significant. The initial condition of a uniform bulk concentration is therefore fails. The experiment was performed five times. Bubble images were processed after the runs to obtain the surface tension evolution (γ) and surface area (A).

3. Theoretical framework

The bubble deformation and associated fluid flow are assumed to die out rapidly compared to the time required for surfactant to restore its equilibrium distribution. Deviations of the bubble shape from a spherical geometry are slight, and are neglected in the analysis. Therefore, surfactant is assumed to diffuse through a quiescent fluid to adsorb on the bubble interface. The solution to Fick's equations for this geometry is a Ward and Tordai equation modified to account for the spherical shape of the bubble [9].

$$\Gamma(t) = \Gamma_b + 2(D/\pi)^{1/2}\left[C_\infty t^{1/2} - \int_0^{\sqrt{t}} C_s(t-\tau)\mathrm{d}\tau^{1/2}\right] + (D/b)\left[C_\infty t - \int_0^t C_\infty(\tau)\mathrm{d}\tau\right] \quad (1)$$

where D denotes the diffusion coefficient, $C_s(t)$ is the subsurface concentration, $\Gamma(t)$ is the surface concentration, Γ_b is the initial surface concentration, b is the bubble radius, and C_∞ is the bulk concentration far from the interface.

The generalized Frumkin (GF) model is adopted to describe the rates of adsorption and desorption. Adsorption and desorption are assumed to be activated processes [11,12] with activation energies for adsorption (E_a) and desorption (E_d) that depend on Γ by a power law [9]:

$$E_a = E_a^0 + RTv_a^*(\Gamma/\Gamma_\infty)^n \qquad E_d = E_d^0 + RTv_d^*(\Gamma/\Gamma_\infty)^n \quad (2)$$

where E_a^0, E_d^0, v_a^*, v_d^*, and n are constants, and RT is the product of the ideal gas constant and the absolute temperature. These adsorption energies weight the kinetic constants for adsorption (β_0) and desorption (α_0) at infinite dilution:

$$\beta = \beta_0 \exp(-E_a/RT) = \beta_1 \exp\left(-v_a^* \frac{\Gamma^n}{\Gamma_\infty^n}\right)$$
$$\alpha = \alpha_0 \exp(-E_d/RT) = \alpha_1 \exp\left(-v_d^* \frac{\Gamma^n}{\Gamma_\infty^n}\right) \quad (3a)$$

where the kinetic constants are recast in terms of

$$\beta_1 = \beta_0 \exp(-E_a^0/RT)$$

and

$$\alpha_1 = \alpha_0 \exp(-E_d^0/RT) \quad (3b)$$

to make the dependence on Γ explicit. Finally, intermolecular interactions are assumed to alter the rate of desorption, but leave the rate of adsorption unaffected, so v_a^* is assumed to be zero. With these assumptions, the adsorption flux to the interface is assumed to obey:

$$\frac{d\Gamma}{dt} = \beta_1 C_s(\Gamma_\infty - \Gamma) - \alpha_1 \exp\left(-v_d^* \frac{\Gamma^n}{\Gamma_\infty^n}\right)\Gamma \quad (4)$$

where C_s is the sublayer concentration, or the concentration of surfactant immediately adjacent to the interface that has yet to adsorb. At equilibrium, the surface concentration which reduces at equilibrium to the isotherm:

$$\frac{\Gamma_{eq}}{\Gamma_\infty} = x = \frac{C_\infty}{C_\infty + a \exp(Kx^n)} \quad (5)$$

where Γ_∞ is the maximum packing at the interface, $1/a = \beta_1/\alpha_1$ is a measure of the surface activity at the interface, and the interaction parameter K is given by:

$$K = v_a^* - v_d^* \quad (6)$$

Attractive intermolecular forces, such as van der Waal's attractions among the hydrocarbon chains of the surfactant, are described by $K < 0$ [5,13]. For this case, the greater is the surface concentration, the slower is the desorption rate. A positive K indicates an anti-cooperative adsorption, which the adsorption becomes more difficult at increasing Γ [1,4]. Eq. (5) becomes the Frumkin isotherm [9,14–17] when a linear dependence between $E_{a/d}$ and Γ is assumed. The Langmuir adsorption isotherm results when $E_{a/d}$ is independent of Γ.

Assuming an ideal bulk solution, the Gibbs adsorption equation allows the derivation of the surface equation of state relating the surface tension γ to the surface concentration:

$$\gamma - \gamma_0 = \Gamma_\infty RT[\ln(1-x) - Knx^{n+1}/(n+1)] \quad (7)$$

where γ_0 is the surface tension of the interface is the absence of surfactants.

When diffusion from the bulk to the interface is slow compared to the rates of adsorption and desorption, diffusion is the rate limiting process. Diffusion supplies the sublayer, and surfactant rapidly establishes equilibrium between the sublayer and the interface. The surface concentration therefore evolves according to Eq. (1) and the isotherm requiring equilibrium between the Γ and C_s:

$$\frac{\Gamma(t)}{\Gamma_\infty} = \frac{C_s(t)}{C_s(t) + a \exp\left(K \frac{\Gamma(t)^n}{\Gamma_\infty^n}\right)} \quad (8)$$

When the rate that surfactant diffuses to the interface is comparable to the rates of adsorption–desorption, the mass transfer is of mixed control, and $\Gamma(t)$ is found by solving Eqs. (1) and (4) simultaneously. The surface tension is assumed to instantaneously reflect the adsorbed concentration in all cases, so $\gamma(\Gamma(t))$ is found from Eq. (7).

Intermolecular interactions among the adsorbed surfactants play an important role in the equilibrium and dynamic data.

Data are analyzed both in terms of the GF and the Frumkin (F) model, for which $n = 1$. Because these models give slightly different relationships between Γ and C_s, slightly different values for diffusivities D and kinetic constants β_1 and α_1 result. Both are reported and compared to results for other members of the homologous series C_mE_8. The best-fit parameters for the GF and F equilibrium models for the surfactants discussed in this paper are given in Table 1. The adsorption of $C_{14}E_8$ onto a freshly created air–water interface has been shown to be of diffusion control with a fixed diffusion coefficient over the concentration range from Lin et al. [8] The diffusion coefficient was obtained by comparing diffusion-controlled predictions to the evolution of pendant bubble

Table 1
Model parameters, diffusivity and kinetic rate constants of C_mE_8

m	Model[a]	$\Gamma_\infty \times 10^{10}$ (mol cm^{-2})	a (mol cm^{-3})	K	n	$D \times 10^6$ cm^2 s^{-1}	$\beta_1 \times 10^{-6}$ cm^3 (mol s)$^{-1}$	α_1 (s^{-1})
14	F	6.800	1.150×10^{-11}	14.0		9.8		
12	F	2.668	2.501×10^{-11}	5.19				
10	F	3.070	1.302×10^{-10}	9.63				
14	GF	4.951	1.128×10^{-13}	12.20	0.3848	7.6	5.4	6.1×10^{-7}
12	GF	5.282	2.329×10^{-12}	13.23	0.532	8.0	4.6	1.1×10^{-5}
10	GF	3.424	2.13×10^{-11}	10.88	0.556	6.5	6.9	1.5×10^{-4}

[a] F, Frumkin; GF, generalized Frumkin.

data for both the F and GF models ($D = 9.8 \times 10^{-6}$ and 7.6×10^{-6} cm^2 s^{-1} for the F and GF models, respectively). These diffusivities were used in the following calculation.

4. Results

Before being impulsively compressed or expanded, the bubble, of surface area A_{eq}, is at equilibrium with the surrounding surfactant solution, with surface tension γ_{eq}, and surface concentration Γ_{eq}. The bubble is then rapidly compressed or expanded to attain a surface tension value of γ_b with surface area A_b and surface coverage is Γ_b. Post expansion or compression, the surfactant begins to redistribute by mass transfer from or to the interface from the non-equilibrium surface concentration Γ_b to re-establish equilibrium.

4.1. Compression

Representative evolution profiles for the surface tension (circles) and surface area (triangles) of a pendant bubble which under goes a rapid, non-perturbative compression are shown in Fig. 1. In Fig. 1(a) data obtained for $C_\infty = 1.0 \times 10^{-9}$ mol cm^{-3} are presented. The pendant bubble is initially in equilibrium with the surrounding surfactant solution, with surface tension $\gamma_{eq} = 49.0$ mN m^{-1}. The bubbles is then compressed over 0.13 s, causing the surface tension to decrease to $\gamma_b = 45.16$ mN m^{-1}. (See the point marked L in the figure, corresponding to the lowest surface tension at the end of the surface compression.) The surface tension then increases as surfactant desorbs from the interface and diffuses through the bulk to restore equilibrium, which is attained after roughly 600 s. The decrease in surface area during the compression was 11% in 0.13 s; thereafter, the surface area remains nearly fixed. Another example is shown in Fig. 1(b) for $C_\infty = 3.0 \times 10^{-9}$ mol cm^{-3}. All the surface tensions evolved in a similar manner. The surface tension decreased abruptly during the compression from the equilibrium value

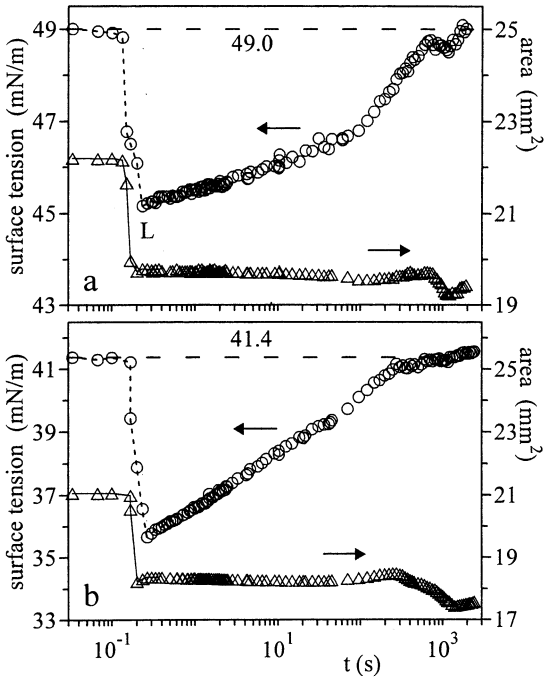

Fig. 1. Representative dynamic surface tensions and surface area of pendant bubble for the re-equilibration process due to a sudden compression of the interface for $C_{14}E_8$ aqueous solution. C_∞ = (a) 1.0 and (b) 3.0 [10^{-9} mol cm^{-3}].

to a lower one and then increased smoothly up to its equilibrium value. The data in Fig. 1 were re-plotted in Fig. 2. The moment with the lowest surface tension (γ_b) was set to be the initial time for comparison to the theoretical simulation of the desorption and diffusion process. The simulation requires an initial surface concentration, Γ_b. This value is extracted from the experiment by using the surface equation of state to find the surface concentration that corresponds to γ_b.

Data in Table 2 (the column of $A_i\Gamma_i/A_e\Gamma_e$, showing the relative amount of $C_{14}E_8$ molecules at bubble surface) indicate that the desorption during the ramp type area change was insignificant for the present system. The desorption of $C_{14}E_8$ molecules during the compression process was therefore neglected in the following simulation.

The diffusion-controlled relaxation profiles predicted by the F and GF models are shown in Fig. 2 (the dashed curves, marked DC in the figure). The DC results from both models depart significantly from the dynamic $\gamma(t)$ data as the bulk concentration is increased. For the runs with $C_\infty = 1.0 \times 10^{-9}$ mol cm^{-3}, departures from DC are slight. (The data at this concentration are compared to simulation for the F model in Fig. 2(a) and the GF model in Fig. 2(c).) When the C_∞ is increased to 3.0×10^{-9} mol cm^{-3}, the departures become more pronounced. (See Fig. 2(b) for comparison to the F model and Fig. 2(d) for comparison to the GF model, respectively.) Theoretical surface tension evolutions assuming mixed control are also compared to the data in Fig. 2 (the solid curves). The adsorption rate constant (β_1) which best describes the data is about the same for different runs at different concentrations (as shown in Fig. 3). Average values are obtained for $\beta_1 = 1.6 \times 10^6$ cm^3 (mol s)$^{-1}$ for the F model and $\beta_1 = 5.4 \times 10^6$ cm^3 (mol s)$^{-1}$ for the GF model, respectively.

4.2. Expansion

Next consider the adsorption of $C_{14}E_8$ molecules onto a depleted surface caused by a sudden expansion of the bubble. In Fig. 4, representative profiles of surface tension (circles) and surface

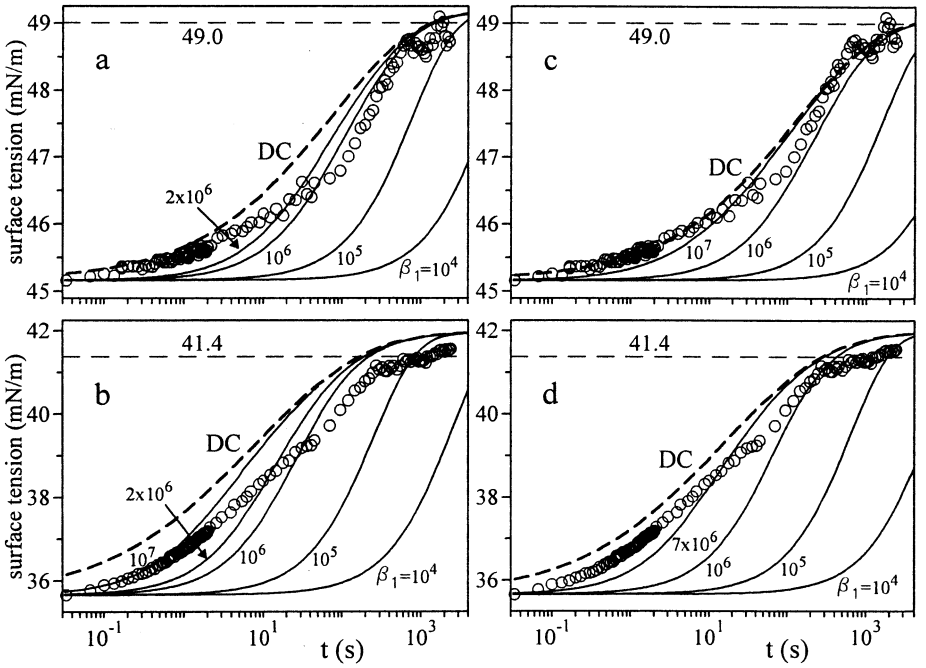

Fig. 2. Dynamic surface tensions and theoretical predictions of diffusion-controlled (dashed curves) and mixed-controlled (solid curves) re-equilibration of the F (a and b) and GF (c and d) models. C_∞ = (a and c) 1.0 and (b and d) 3.0 [10^{-9} mol cm^{-3}].

Table 2
Relaxations of surface properties during the shrinkage of bubble, $C = 1 \times 10^{-9}$ mol cm^{-3}

t (s)	γ (mN m^{-1})	A (mm^2)	A_i/A_e	$\Gamma_i/\Gamma_{\gamma=54}$[a]	$A_i\Gamma_i/A_e\Gamma_e$[a]
−1/30	48.95	22.19	1.00	1.226	1.00
0	48.92[b]	22.19	1.00	1.228	1.00
1/30	48.82[c]	22.15	1.00	1.232	1.00
3/60	46.77[c]	21.66	0.98	1.322	1.05
2/30	46.50[c]	19.97	0.90	1.333	0.98
3/30	46.09[c]	19.74	0.89	1.351	0.98
4/30	45.16[d]	19.80	0.89	1.391	1.01
5/30	45.22	19.79	0.89	1.388	1.01
6/30	45.26	19.77	0.89	1.387	1.01
7/30	45.23	19.78	0.89	1.388	1.01

[a] The relative surface concentration calculated from γ by applying the relationship of γ vs. $\Gamma/\Gamma_{\gamma=54}$, which was obtained from the fast expansion of pendant bubble (Ref. [8]).
[b] The point right before the desorption process, corresponding to the equilibrium state.
[c] The point during the shrinkage of bubble.
[d] The point with the lowest surface tension, corresponding to the end of shrinkage and the beginning of the desorption process.

area (triangles) obtained for a pendant bubble in a surfactant solution of $C_\infty = 2.0 \times 10^{-9}$ mol cm^{-3} are shown. In this example, the surface tension increased from 43.8 mN m^{-1} up to 52.2 mN m^{-1} in 1.26 s. Thereafter, surfactant adsorbs to re-establish equilibrium over roughly 1000 s. The surface area of pendant bubble increased 32% during the expansion and then kept a nearly constant value. All the relaxation data showed a similar behavior. The surface tension increased in about 1.3 s from the equilibrium value to a higher one (indicated by the point H in the figure), corresponding to the end of bubble expansion, and then decreased smoothly down to its equilibrium value.

The data in Fig. 4 were re-plotted in Fig. 5, with the highest surface tension plotted as the initial point for the re-equilibration process. The initial surface concentration for these simulations was calculated from the surface equation of state. Table 3 presents a set of surface properties during

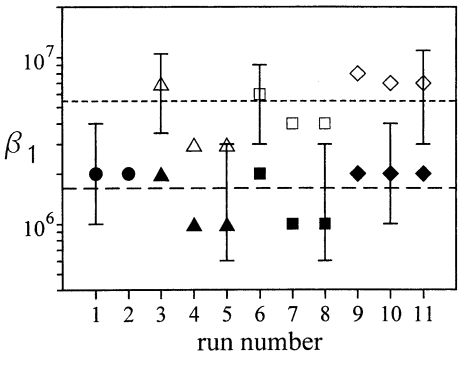

Fig. 3. Values of adsorption rate constant β_1 evaluated from the re-equilibration process due to a sudden compression of the interface using the GF (open marks) and F (filled marks) models. $C_\infty = 1.0$ (○), 1.3 (△), 2.0 (□), and 3.0 (◇) [10^{-9} mol cm^{-3}].

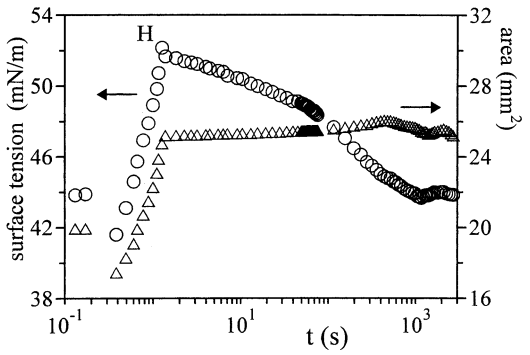

Fig. 4. Representative dynamic surface tensions and surface area of pendant bubble for re-equilibration due to a fast expansion of the interface of $C_{14}E_8$ aqueous solutions for $C_\infty = 2.0 \times 10^{-9}$ mol cm^{-3}.

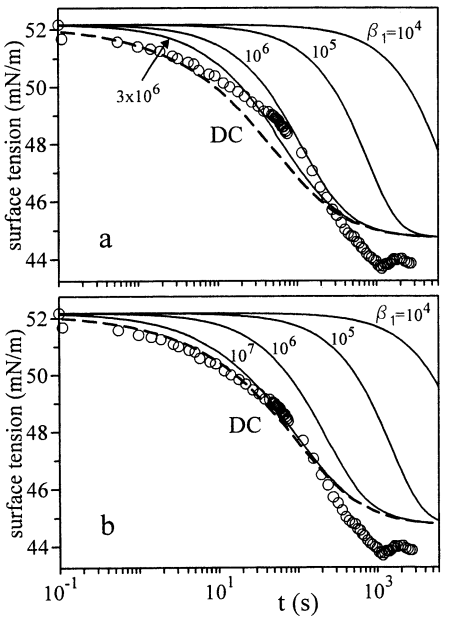

Fig. 5. Dynamic surface tensions and theoretical predictions of diffusion-controlled (dashed curves) and mixed-controlled (solid curves) re-equilibration of the F (a) and GF (b) models. $C_\infty = 2.0 \times 10^{-9}$ mol cm^{-3}.

the bubble expansion. The column of $A_i\Gamma_i/A_e\Gamma_e$, showing the relative amount of $C_{14}E_8$ molecules at surface, indicates that the adsorption during the ramp type area change was nearly negligible for the present system. Therefore, the adsorption during the surface expansion (≈ 1.3 s) was neglected in the following calculation.

The diffusion-controlled evolutions of the surface tension for the re-equilibration process are shown in Fig. 5 as the dashed curves. The theoretical DC profiles from both models agree with the dynamic $\gamma(t)$ data satisfactorily. Theoretical relaxation profiles with a finite adsorption rate constant (β_1) were also calculated and plotted in Fig. 5 (the solid curves). The fit from GF model (Fig. 5(b)) clearly indicates that it is of diffusion control.

The model prediction from the F model is slightly faster than the $\gamma(t)$ data. Therefore it is a mixed-controlled or a nearly diffusion-controlled process. An adsorption rate constant $\beta_1 = 3 \times 10^6$ cm^3 (mol s)$^{-1}$ results from the fit and this β_1 value is nearly the same as that from the surface-compression experiment.

Table 3
Relaxations of surface properties during the expansion of bubble, $C = 2 \times 10^{-9}$ mol cm^{-3}

t (s)	γ (mN m^{-1})	A (mm^2)	A_i/A_e	$\Gamma_i/\Gamma_{\gamma=54}$[a]	$A_i\Gamma_i/A_e\Gamma_e$[a]
	43.80[b]	19.06	1.00	1.448	1.00
0.05	39.74[c]	16.68	0.88	1.610	0.97
0.38	41.60[c]	17.47	0.92	1.538	0.97
0.49	43.11[c]	18.30	0.96	1.477	0.98
0.60	44.59[c]	19.10	1.00	1.415	0.98
0.66	45.74[c]	19.92	1.05	1.366	0.99
0.77	46.94[c]	20.72	1.09	1.314	0.99
0.88	47.90[c]	21.49	1.13	1.273	0.99
0.93	48.93[c]	22.28	1.17	1.227	0.99
1.10	49.84[c]	23.09	1.21	1.187	0.99
1.15	50.74[c]	23.87	1.25	1.147	0.99
1.26	52.17[d]	24.75	1.30	1.083	0.97
1.37	51.68[e]	25.21	1.32	1.105	1.01
1.81	51.58[c]	25.22	1.32	1.109	1.01

[a] The relative surface concentration calculated from γ by applying the relationship of γ vs. $\Gamma/\Gamma_{\gamma=54}$, which was obtained from the fast expansion of pendant bubble (Ref. [8]).
[b] The point right before expansion, corresponding to the equilibrium state.
[c] The point during the expansion of bubble.
[d] The point with the highest surface tension, corresponding to the end of expansion and the beginning of re-equilibration.
[e] The point during the re-equilibration process, surfactants adsorb onto interface.

4.3. Simulation

A theoretical simulation, the same as that in ref [18], was performed to investigate the controlling mechanism for $C_{14}E_8$ on the re-equilibration processes due to the compression and expansion of the air–water interface. The model constants and diffusivity used for the simulation are listed in Table 1. Fig. 6 shows the relationship of β^l vs. C (surfactant concentration). Here, the limiting adsorption rate constant β^l is the lower limit of β_1, with which the relaxation profile of $\gamma(t)$ is indistinguishable from the diffusion-controlled one. Curves C (the circles) and E (the diamonds) are for the re-equilibration processes due to the compression (13% of surface area) and fast expansion (30% of surface area) of air–water interface, respectively.

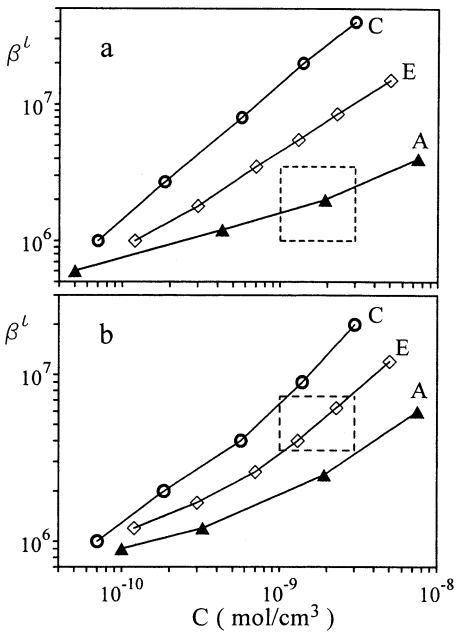

Fig. 6. Limiting adsorption rate constant β^l (cm^3 (mol s)$^{-1}$) as a function of bulk concentration C_∞ as the F (a, $D = 9.8 \times 10^{-6}$ cm^2 s^{-1}) and GF (b, $D = 7.6 \times 10^{-6}$ cm^2 s^{-1}) models are applied for the adsorption onto a clean surface (A), adsorption onto a suddenly expanded surface (E, $A_b/A_e = 1.3$), and a suddenly compressed surface (C, $A_b/A_e = 0.87$).

4.4. Comparison

First consider the case using the F model (Fig. 6(a)), β^l increases from 1×10^6 to 4×10^7 cm^3 (mol s)$^{-1}$ for curve C and from 1×10^6 to 1.5×10^7 cm^3 (mol s)$^{-1}$ for curve E. Therefore, there exists a possibility for both re-equilibration processes to be of diffusion controlled at dilute concentration and shift to a diffusive-kinetic mixed controlled process at more elevated concentrations. Values of β_1 evaluated from the desorption experiment (Fig. 3) are plotted in Fig. 6 as a broken rectangular box at the experimental concentration range in this work. Curves C and E are above the broken box at $C_\infty > 1 \times 10^{-9}$ mol cm^{-3}. This indicates that both re-equilibration processes should be mixed controlled at the working concentrations ($1–3 \times 10^{-9}$ mol cm^{-3}) in this study. Experimental data agree well with the simulation results: the desorption due to a sudden surface compression is of mixed control (Fig. 2) and the adsorption due to a fast surface expansion is mixed but nearly diffusion controlled (Fig. 5(a)). Note that the adsorption onto a freshly created surface had been confirmed to be a diffusion-controlled process [8]. Curve A in Fig. 6(a) indicates that the adsorption is of diffusion-control at $C_\infty < 3 \times 10^{-9}$ mol cm^{-3} and it is diffusion-controlled or nearly diffusion-controlled at $3 \times 10^{-9} < C_\infty < 8 \times 10^{-9}$ mol cm^{-3}.

If one applies the GF model, β^l increases from 1×10^6 to 2×10^7 cm^3 (mol s)$^{-1}$ for curve C and from 1×10^6 to 1.2×10^7 cm^3 (mol s)$^{-1}$ for curve E (Fig. 6(b)). Experimental results of β_1 (the broken rectangular box for the working concentrations in this work) imply that the re-equilibration process due to the fast surface-compression will be diffusion-controlled at dilute concentrations ($C_\infty < 5 \times 10^{-10}$ mol cm^{-3}) and shift to be mixed controlled at $C_\infty > 1 \times 10^{-9}$ mol cm^{-3}. Since the concentration used for the compression experiment is $1–3$ ($\times 10^{-9}$ mol cm^{-3}), therefore it is found that the desorption due to a sudden surface compression is of mixed control (Fig. 2). A similar shift in the controlling mechanism exists for the re-equilibration process due to a fast surface expansion. Due to the working concentration is 2×10^{-9} mol cm^{-3} in this study, this

process is found to be diffusion-controlled (Fig. 5(b)) for the runs in this work.

5. Comparison of C_mE_8

The adsorption kinetics of C_mE_8 ($m = 10$, 12, and 14) on a perturbed air–water interface is compared here. The model constants, diffusivity, and kinetic rate constants are listed in Table 1. Only the results from the GF model are discussed below since it predicted the dynamic data generally better than the F model. This was evidenced since the GF model describes better the experimental data of equation of state (Γ vs. γ dependence) [8].

First, the desorption processes for these three C_mE_8 due to a sudden surface compression are all diffusive-kinetic mixed controlled even thought the adsorptions of C_mE_8 onto a clean surface have different mechanisms: diffusion-control for $C_{14}E_8$ and mixed-control for $C_{12}E_8$ and $C_{10}E_8$ [1,2,4,8]. In other words, the rates of bulk diffusion and interfacial adsorption–desorption are of the same order of magnitude, and neither of them can be neglected in the re-equilibration process.

These three C_mE_8 molecules have a nearly same molecular size, therefore, have a nearly same diffusivity ($D = 7.4 \pm 1.0 \times 10^{-6}$ cm^2 s^{-1} by using the GF model, as shown in Table 1). A nearly same value of adsorption rate constant ($\beta_1 = 5.6 \pm 1.0 \times 10^6$ cm^3 (mol s)$^{-1}$, Table 1) is resulted for these three C_mE_8 at 25 °C. However, the desorption rate constant (α_1) varies a lot for C_mE_8: an increase of m by 2 lowers the value of α_1 about 15 times. The straight hydrocarbon chains result strong van der Waal's forces between the adsorbed C_mE_8 molecules. The molecules with longer hydrocarbon chains must overcome stronger attractive forces on leaving the interfacial monolayer and desorbing onto the aqueous bulk phase. Therefore $C_{14}E_8$ has the lowest α_1 and $C_{10}E_8$ has the highest α_1.

A quite different trend on the rate constants was reported by Fainerman and Lylyk [19] for aqueous alcohols solutions C_mOH ($m = 4$–7). The F model was applied and they obtained a nearly same desorption rate constant ($\alpha_1 = 110 \pm 10$ s^{-1}; $\alpha_1 =$ 105, 110, 102 and 119 s^{-1} for $m = 3$, 4, 5 and 6, respectively) for these four alcohols and the adsorption rate constant increases 10 times when m increases 2 [$\beta_1 = 1$, 3, 10 and 30 (10^7 cm^3 (mol s)$^{-1}$) for $m = 4$, 5, 6 and 7, respectively]. More rate constant data of nonionic surfactants are listed in Ref. [20].

6. Discussion and conclusions

If $C_{14}E_8$ does follow what the (generalized) Frumkin model predicts, the mass transport of $C_{14}E_8$ in a quiescent surfactant solution on a perturbed air–water interface should be diffusion-controlled at dilute concentrations and diffusive–kinetic mixed controlled at more elevated bulk concentrations. Note that at the working concentrations in this study, the desorption is mixed controlled and the adsorption due to a sudden surface expansion is (nearly) diffusion controlled. The sorption constant at 25 °C evaluated from the experimental data are $\beta_1 = 5.4 \times 10^6$ cm^3 (mol s)$^{-1}$, $\alpha_1 = 6.1 \times 10^{-7}$ s^{-1} using the GF model.

When the dynamic $\gamma(t)$ data for the adsorption onto a freshly created surface are unavailable and one try to use the $\gamma(t)$ data of the re-equilibration processes on a perturbed air–water interface to study the adsorption kinetics, for example, the oscillating bubble technique. Commonly, one assumes firstly the process is diffusion-controlled and checks the fit between the $\gamma(t)$ data and model prediction and the value of diffusivity. If the fit is satisfactorily and the diffusivity is closed to what the Stokes–Einstein equation predicts, one will conclude that it is a diffusion-controlled process.

To examine the above procedure, the dynamic $\gamma(t)$ data of re-equilibration due to a sudden surface compression are fitted with theoretical profiles of diffusion-control with different diffusivities. Fig. 7 shows two examples for $C_\infty = 1.3$ and 2.0×10^{-9} mol cm^{-3} using the F and GF models. It is interesting to find that the fits between the $\gamma(t)$ data and diffusion-controlled profiles are nearly perfect and a nearly constant diffusivity is resulted (as shown in Fig. 8). $D =$ 2.5 ± 0.6 and 3.4 ± 0.3 (10^{-6} cm^2 s^{-1}) by applying the F and GF models, respectively. Similar results

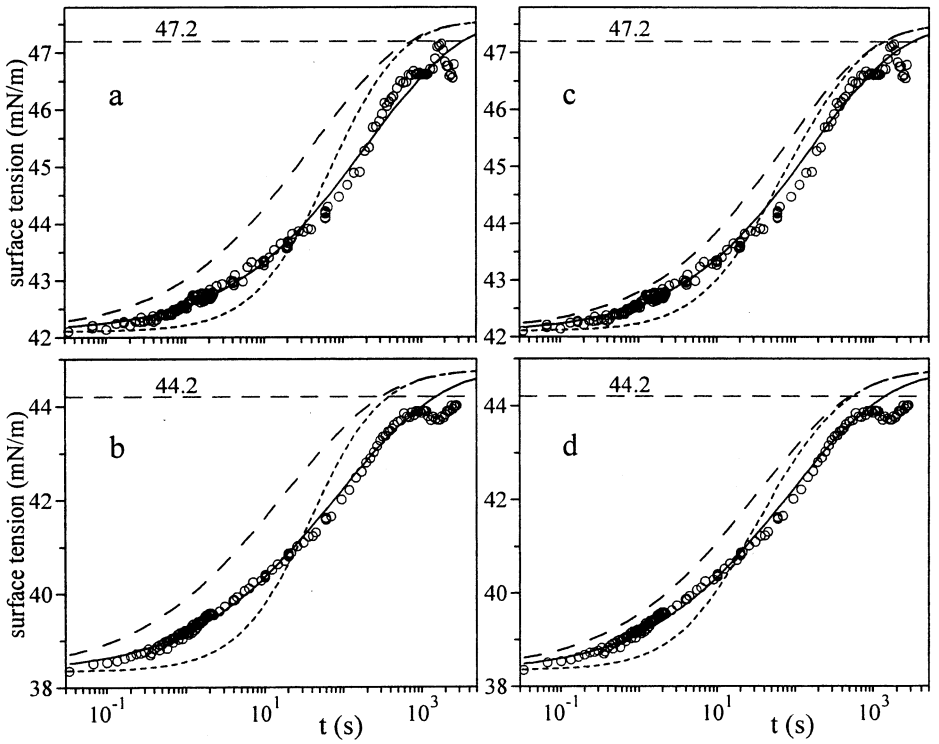

Fig. 7. Experimental dynamic surface tension for the re-equilibration of $C_{14}E_8$ and the theoretical predictions of diffusion controlled profiles with different diffusivities using the F (a and b) and GF (c and d) models. $C_\infty = 1.3$ (a and c) and 2.0 (b and d) [10^{-9} mol cm^{-3}]. $D = 9.8 \times 10^{-6}$ (dashed curves in a and b), 2.0×10^{-6} (solid curves in a and b), 7.6×10^{-6} (dashed curves in c and d), 3.0×10^{-6} and 3.5×10^{-6} (solid curves in c and d, respectively) cm^2 s^{-1}. The dotted curves are the best-fit of mixed controlled process.

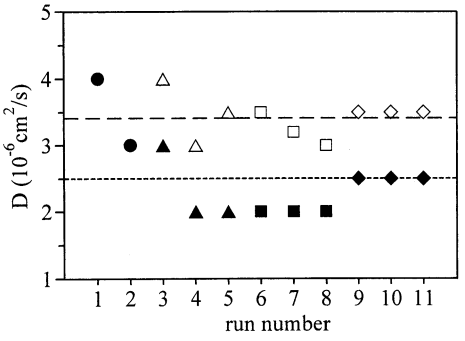

Fig. 8. Diffusivities obtained from the desorption experimental data by assuming the process is diffusion controlled and using the GF (open marks) and F (filled marks) models. $C_\infty = 1.0$ (○), 1.3 (△), 2.0 (□), and 3.0 (◇) [10^{-9} mol cm^{-3}].

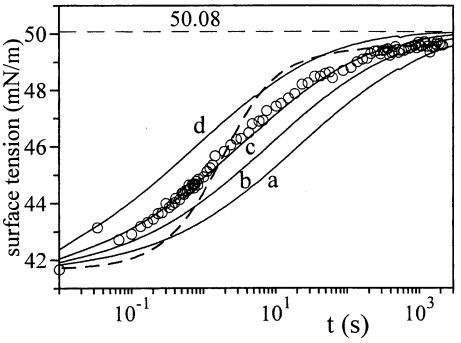

Fig. 9. Experimental dynamic surface tension for the re-equilibration of $C_{12}E_8$ and the theoretical diffusion-controlled predictions with different diffusivities using the GF model. $C_\infty = 7.32 \times 10^{-9}$ mol cm^{-3}, D = (a) 0.30; (b) 0.80; (c) 2.0 and (d) 8.0 ($\times 10^{-6}$ cm^2 s^{-1}). The dotted curves are the best-fit of mixed controlled process.

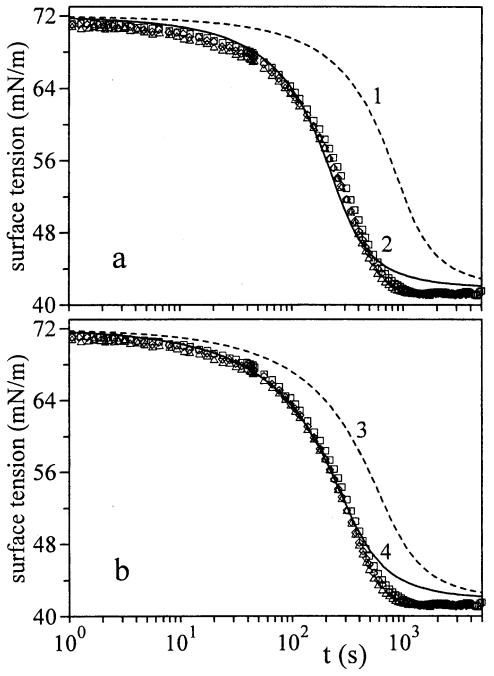

Fig. 10. Experimental dynamic surface tension (mN m^{-1}) for the adsorption of $C_{14}E_8$ ($C_\infty = 3.0 \times 10^{-9}$ mol cm^{-3}) onto a fresh surface and the theoretical profiles of diffusion control of the F (a) and GF (b) models for $D = 2.5$ (1), 9.5 (2), 3.4 (3) and 7.5 (4) [10^{-6} cm^2 s^{-1}].

were also observed for $C_{12}E_8$ and $C_{10}E_8$. A representative example is shown in Fig. 9. Nearly constant diffusivities ($D = 2.0 \times 10^{-6}$ cm^2 s^{-1} for $C_{12}E_8$ and 3.0×10^{-6} cm^2 s^{-1} for $C_{10}E_8$) were also resulted from the dynamic re-equilibration $\gamma(t)$ data and the GF model.

However, the model predictions for the adsorption of $C_{14}E_8$ onto a fresh surface with $D = 2.5 \times 10^{-6}$ cm^2 s^{-1} (F model) and 3.4×10^{-6} cm^2 s^{-1} (GF model) are far from the dynamic surface tension data (Fig. 10). Unless C_mE_8 molecules aggregate at interface and also mass-transport in clusters at the bulk phase and at air–water interface, otherwise, the diffusivity has no chance to lower to 2–3.5 (10^{-6} cm^2 s^{-1}). The desorption of $C_{14}E_8$ out of the suddenly compressed surface is therefore mixed controlled.

Acknowledgements

This work was supported by the National Science Council of Taiwan, Republic of China (Grant NSC 89-2214-E-011-021).

References

[1] S.Y. Lin, R.Y. Tsay, L.W. Lin, S.I. Chen, Langmuir 12 (1996) 6530.
[2] R.Y. Tsay, S.Y. Lin, L.W. Lin, S.I. Chen, Langmuir 13 (1997) 3191.
[3] J. Eastoe, J.S. Dalton, P.G.A. Rogueda, E.R. Crooks, A.R. Pitt, E.A. Simister, J. Colloid Interf. Sci. 188 (1997) 423.
[4] H.C. Chang, C.T. Hsu, S.Y. Lin, Langmuir 14 (1998) 2476.
[5] R. Pan, J. Green, C. Maldarelli, J. Colloid Interf. Sci. 205 (1998) 213.
[6] B. Li, G. Geeraerts, P. Joos, Colloids Surfaces 88 (1994) 251.
[7] G. Loglio, U. Tesei, R. Miller, R. Cini, Colloids Surfaces 61 (1991) 219.
[8] S.Y. Lin, Y.C. Lee, M.J. Shao, C.T. Hsu, J. Colloid Interf. Sci. 244 (2001) 372.
[9] S.Y. Lin, K. McKeigue, C. Maldarelli, Langmuir 7 (1991) 1055.
[10] S.Y. Lin, L.J. Chen, J.W. Xyu, W.J. Wang, Langmuir 11 (1995) 4159.
[11] S.S. Dukhin, G. Kretzschmar, R. Miller, Dynamics of Adsorption at Liquid Interfaces, Elsevier, 1995.
[12] R. Aveyard, D.A. Haydon, An Introduction to the Principles of Surface Chemistry (Chapters 1 and 3), Cambridge University Press, Cambridge, 1973.
[13] D.O. Johnson, K.J. Stebe, J. Colloid Interf. Sci. 182 (1996) 526.
[14] A. Frumkin, Z. Phys. Chem. (Leipzig) 116 (1925) 466.
[15] C.H. Chang, E.I. Franses, Colloids Surfaces 69 (1992) 189.
[16] H. Diamant, D. Andelman, Europhys. Lett. 34 (1996) 575.
[17] R.P. Borwankar, D.T. Wasan, Chem. Eng. Sci. 38 (1983) 1637.
[18] C.T. Hsu, S.Y. Lin, J. Chin. Inst. Chem. Eng. 29 (1998) 129.
[19] V.B. Fainerman, S.V. Lylyk, Kolloidn. Zh. 44 (1982) 598.
[20] K.J. Stebe, S.Y. Lin, Dynamic surface tension and surfactant mass transfer kinetics: measurement techniques and analysis, in: H.S. Nalwa (Ed.), Handbook of Surfaces and Interfaces of Materials, vol. 2, Academic Press, San Diego, 2001.